Removal of NO_x and NO_y in biomass burning plumes in the boundary layer over northern Australia

N. Takegawa,[1] Y. Kondo,[1] M. Koike,[2] M. Ko,[3,4] K. Kita,[5] D. R. Blake,[6] N. Nishi,[7] W. Hu,[8] J. B. Liley,[9] S. Kawakami,[10] T. Shirai,[10] Y. Miyazaki,[1] H. Ikeda,[1] J. Russel-Smith,[11] and T. Ogawa[10]

Received 4 May 2002; revised 5 November 2002; accepted 20 November 2002; published 22 May 2003.

[1] The Biomass Burning and Lightning Experiment Phase B (BIBLE-B) aircraft measurement campaign was conducted over the western Pacific and Australia in August and September 1999. In situ aircraft measurements of carbon monoxide (CO), nitric oxide (NO), total reactive nitrogen (NO_y), ozone (O_3), nonmethane hydrocarbons (NMHCs), and other species were made during BIBLE-B. Meteorological analysis shows that the trace gases emitted from biomass burning in northern Australia were mostly confined within the planetary boundary layer (below ~3 km) by strong subsidence in the free troposphere. Removal processes of NO_x (equal to measured NO + calculated NO_2) and NO_y in biomass burning plumes in the boundary layer are examined on the basis of correlation analysis. The photochemical lifetime of NO_x in biomass burning plumes during the daytime is estimated to be 0.1 to 0.3 days using the correlations of NO_x with short-lived NMHCs and hydroxyl radical (OH) concentration calculated from a constrained photochemical model. Correlation of NO_y with CO shows that ~60% of the NO_y molecules originating from biomass burning were removed in the boundary layer within 2–3 days. This result is consistent with dry deposition of nitric acid (HNO_3) in the plumes. It is likely that only a small fraction of NO_y emitted from biomass burning was exported from the boundary layer to the free troposphere during the BIBLE-B period. *INDEX TERMS:* 0322 Atmospheric Composition and Structure: Constituent sources and sinks; 0365 Atmospheric Composition and Structure: Troposphere—composition and chemistry; 0368 Atmospheric Composition and Structure: Troposphere—constituent transport and chemistry; *KEYWORDS:* biomass burning, northern Australia, NO_x lifetime, dry deposition of NO_y

Citation: Takegawa, N., et al., Removal of NO_x and NO_y in biomass burning plumes in the boundary layer over northern Australia, *J. Geophys. Res.*, *108*(D10), 4308, doi:10.1029/2002JD002505, 2003.

1. Introduction

[2] The importance of biomass burning during the tropical dry season is widely recognized, as it has significant impacts on the distributions of ozone (O_3) and its precursors in the troposphere [*Crutzen et al.*, 1979; *Crutzen and Andreae*, 1990]. Several intensive aircraft measurement campaigns have been conducted near the Amazon and southern Africa: Amazon Boundary Layer Experiment-2A (ABLE-2A) [*Harriss et al.*, 1988], Chemical Instrumentation Test and Evaluation 3 (CITE 3) [*Hoell et al.*, 1993], Transport and Atmospheric Chemistry Near the Equator-Atlantic (TRACE-A) [*Fishman et al.*, 1996], and Southern African Fire Atmospheric Research Initiative 1992 (SAFARI 92) [*Lindesay et al.*, 1996]. Chemical characteristics of biomass burning plumes from the Amazon and southern Africa were examined based on the extensive data set obtained during these measurement campaigns. In contrast, only a few intensive measurements of trace gases over Southeast Asia or northern Australia have yet been reported [*Hurst et al.*, 1994; *Matsueda and Inoue*, 1999; *Sawa et al.*, 1999]. Although these measurements have provided useful information on the emission ratios of trace gases over Indonesia and northern Australia, detailed mechanisms of the photochemical and transport processes in this region are not fully understood.

[3] The Biomass Burning and Lightning Experiment - Phase B (BIBLE-B) was conducted over the western Pacific

[1]Research Center for Advanced Science and Technology, University of Tokyo, Tokyo, Japan.
[2]Department of Earth and Planetary Science, University of Tokyo, Tokyo, Japan.
[3]Atmospheric and Environmental Research Inc., Lexington, Massachusetts, USA.
[4]Now at NASA Langley Research Center, Hampton, Virginia, USA.
[5]Department of Environmental Sciences, Ibaraki University, Ibaraki, Japan.
[6]Department of Chemistry, University of California, Irvine, California, USA.
[7]Department of Earth and Planetary Science, Kyoto University, Kyoto, Japan.
[8]Department of Environmental Quality, Richmond, Virginia, USA.
[9]National Institute of Water and Atmosphere, Lauder, New Zealand.
[10]Earth Observation Research Center, National Space Development Agency of Japan, Tokyo, Japan.
[11]Bushfire Council of Northern Territory, Darwin, Northern Territory, Australia.

0148-0227/03/2002JD002505$09.00

Table 1. Characteristics of the Measurements Used in This Study

Species	Sampling interval	Precision[a]	Accuracy
CO	1 s	1 ppbv	5%
NO	1 s	2 pptv	8%
NO_y	1 s	5 pptv	17%
O_3	1 s	0.6 ppbv	5%
J_{NO2}	1 s	1%	8%
NMHCs (C_2-C_{10})	5 min	1–3%	5–10%

[a]Precisions of CO, NO, NO_y, O_3, and J_{NO2} measurements were estimated using 10-s averaged data.

and Australia in August and September 1999 [*Kondo et al.*, 2002], focusing on savanna fires (bushfires) in northern Australia during the middle of the dry season [*Russell-Smith et al*., 2003]. In this paper we investigate the photochemical and transport processes of biomass burning plumes in the boundary layer over northern Australia based on correlation analysis. Specifically, we focus on the removal process of reactive nitrogen, which plays a critical role in atmospheric photochemistry. Meteorological conditions during BIBLE-B are described in sections 3 and 4, and the method of analysis is described in sections 5 and 6. Changes in the correlations among trace gases are discussed in section 7 to estimate the removal rates of reactive nitrogen in biomass burning plumes.

2. Aircraft Measurements

[4] In situ measurements of trace gases were made onboard the Gulfstream-II (G-II) aircraft during BIBLE-B. The measurements used in this study are summarized in Table 1. Because details of the measurements are presented in each of the referenced papers, only important points are described here. Carbon monoxide (CO) was measured using a vacuum ultraviolet (VUV) resonance fluorescence technique [*Takegawa et al.*, 2001]. Nitric oxide (NO) and total reactive nitrogen (NO_y = NO + nitric dioxide (NO_2) + nitric acid (HNO_3) + peroxyacetyl nitrate (PAN) +...) were measured using a NO-O_3 chemiluminescence technique [*Kondo et al.*, 1997; *Koike et al.*, 2000]. The NO_y compounds are catalytically converted to NO with the addition of CO on the surface of a gold tube heated to 300° ± 1°C. O_3 was measured using a dual-beam UV photometer [*Kita et al.*, 2002]. The NO_2 photolysis frequency (J_{NO2}) was measured using uplooking and downlooking filter radiometers (Meteorologie Consult) [*Kita et al.*, 2002]. Nonmethane hydrocarbons (NMHCs) measurements were made by whole air sampling [*Blake et al.*, 1996] with 5-min resolution on average. The photostationary state NO_2 concentrations were calculated using a photochemical box model developed at Atmospheric Environmental Research Inc. (AER) [*Ko et al.*, 2002]. The reactions of NO with O_3, hydroperoxyl radical (HO_2), methylperoxyl radical (CH_3O_2), and ethylperoxyl radical ($C_2H_5O_2$) were taken into consideration. The sum of measured NO and calculated NO_2 was given as NO_x. The precision and accuracy of the 10-s NO_x data were estimated to be 4 pptv and 20%, respectively. The 10-s merged data were used for our analysis of CO, NO_x (= NO + NO_2), NO_y, and O_3. The data that were averaged in accordance with the integration time of NMHC sampling (40–60 s in the boundary layer) were also used for the analysis that included NMHCs.

[5] Figure 1 displays the flight tracks of the G-II during BIBLE-B, together with locations of biomass burning hot spots observed by the Advanced Very High Resolution Radiometer (AVHRR) and the Along Track Scanning Radiometer (ATSR) (http://shark1.esrin.esa.it/ionia/FIRE/AF/ATSR/). The AVHRR is carried onboard the National Oceanic and Atmospheric Administration (NOAA) polar-orbiting satellites, and the data presented here were processed by the Department of Land Administration (DOLA) of Western Australia (http://www.dola.wa.gov.au). The G-II was based in Darwin (12°S, 131°E). Eight flights were conducted over Australia between 31 August and 13 September 1999. Our analysis uses the data collected over Arnhem Land (10°–16°S, 129°–136°E), in the vicinity of Cairns (16°–17°S, 146°–148°E), and over the Timor Sea (14°S, 122°–124°E).

3. Meteorological Conditions During Bible-B

[6] Reanalysis data from the National Centers for Environmental Prediction (NCEP) (http://www.ncep.noaa.gov/)

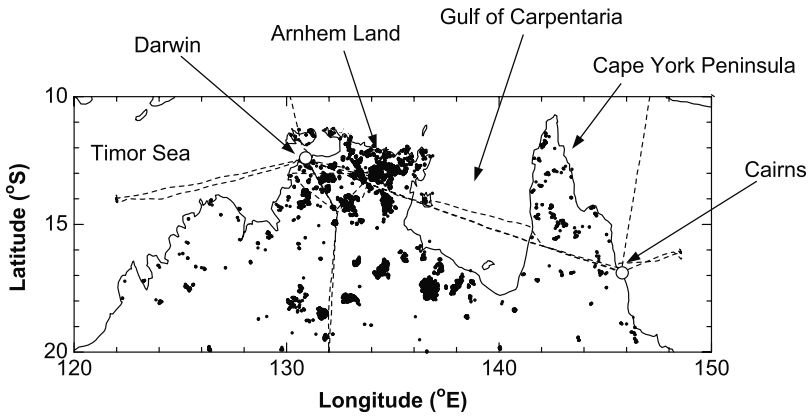

Figure 1. Flight tracks of the Gulfstream-II aircraft during the BIBLE-B campaign over northern Australia (dashed lines). Dots show locations of biomass burning hot spots during BIBLE-B observed from the Advanced Very High Resolution Radiometer (AVHRR) and the Along Track Scanning Radiometer (ATSR).

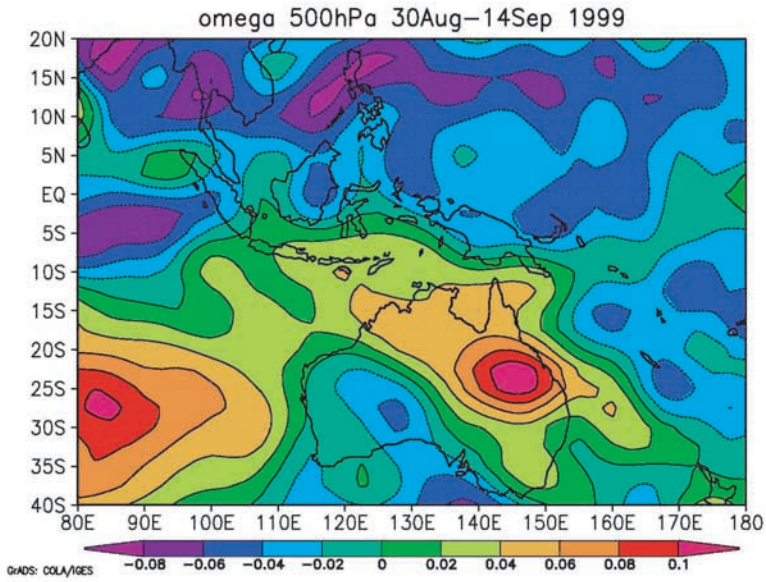

Figure 2. Mean vertical wind (Pa s^{-1}) at 500 hPa (~5.5 km) between 30 August and 14 September 1999. Positive values (warm colors) represent downward motion, and negative values (cold colors) represent upward motion. Note that 0.05 Pa s^{-1} corresponds to ~0.7 km day^{-1}.

were used to examine the meteorological conditions over northern Australia during BIBLE-B. The winds in the lower troposphere (below ~4 km) were dominated by a subtropical high-pressure system centered at 20°–30°S. The mean zonal wind directions below 4 km were generally easterly or southeasterly, and the zonal wind speeds at 850 hPa (~1.5 km) were typically less than ~10 m s^{-1}. The winds in the middle and upper troposphere (above ~4 km) were strongly influenced by a high-pressure system located over northwest Australia. The mean zonal wind directions above 4 km were roughly westerly, but changed frequently as this high-pressure system moved. Figure 2 depicts the mean vertical wind (Pa s^{-1}) at 500 hPa (~5.5 km) between 30 August and 14 September, produced from the NCEP reanalysis data. Downward motions were predominant throughout the middle and upper troposphere over northern Australia during BIBLE-B. The vertical wind speeds were considerable, approximately 0.05 Pa s^{-1} (~0.7 km day^{-1}) at 500 hPa (~5.5 km). These wind fields are similar to those averaged for September of 1979–1995.

[7] Figure 3 shows the monthly burned area in the western part of Arnhem Land (12°–14°S, 133°–134.5°E) and the 3-day running mean of the Outgoing Long-wave Radiation (OLR) averaged for 5°–17.5°S and 120°–150°E. The burned area data were measured by the Bushfire Council of Northern Territory (BFC) [*Russell-Smith et al.*, 2003]. The OLR data observed from the NOAA polar-orbiting satellites [*Liebmann and Smith*, 1996] have been used as a good proxy for tropical deep convection [e.g., *Wheeler and Kiladis*, 1999]. The OLR values during BIBLE-B were close to those averaged for September 1979–1998. The OLR values during BIBLE-B larger than those in November–May (wet season) represent less cloud, consistent with the dominant downward motions in the free troposphere during this period (Figure 2). The BIBLE-B campaign was conducted during a period when the biomass burning activity was near the annual maximum and the convective activity was very weak. Indeed, the precipitation over Arnhem Land was very scarce during BIBLE-B, according

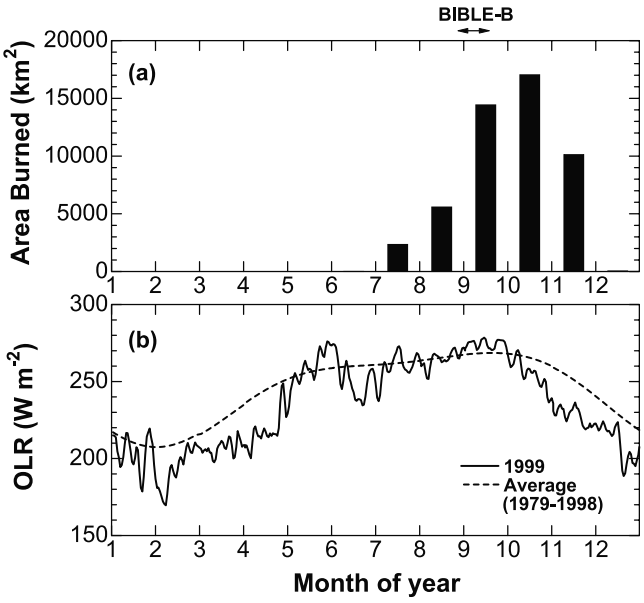

Figure 3. (a) Monthly burned area in the western part of Arnhem Land (12°–14°S, 133°–134.5°E). (b) 3-day running mean of the Outgoing Long-wave Radiation (OLR) data averaged for 5°–17.5°S and 120°–150°E (solid line). The average value for the period 1979–1998 is shown as a dashed line.

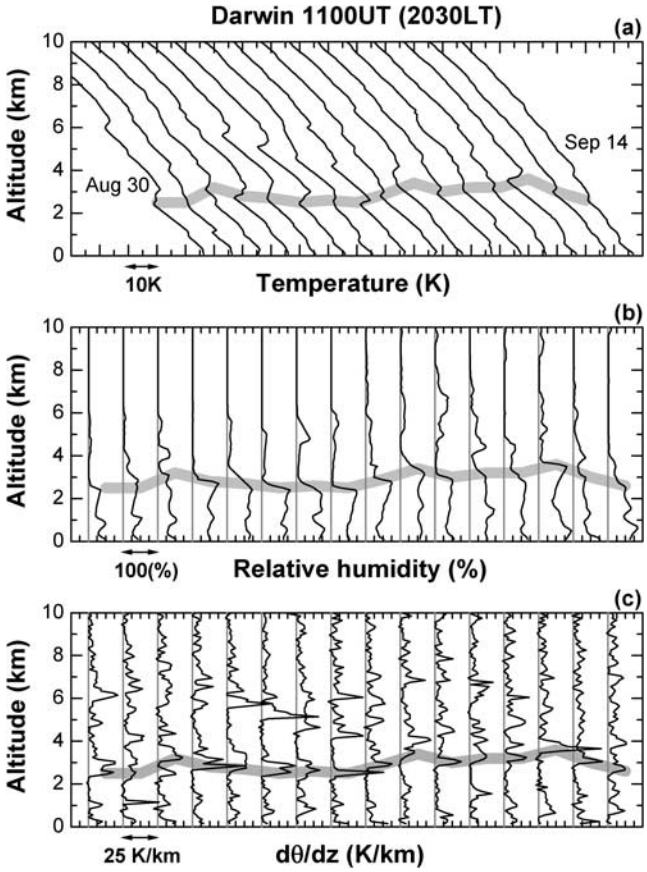

Figure 4. Day-by-day series of the vertical profiles of (a) temperature, (b) relative humidity, and (c) potential temperature gradient ($d\theta/dz$) between 30 August and 14 September obtained by radiosonde soundings over Darwin at 1100 UT (2030 LT). Each profile is shifted for clarity. The top of the planetary boundary layer (PBL) is indicated by the shaded line.

to a report of the Bureau of Meteorology Research Centre (http://www.bom.gov.au/bmrc/).

4. Boundary Layer Over Northern Australia

[8] Figure 4 shows day-by-day series of vertical profiles of temperature (T), relative humidity (RH), and potential temperature gradient ($d\theta/dz$) between 30 August and 14 September obtained by radiosonde over Darwin in the local evening (1100 UT, 2030 LT), where θ and z denote the potential temperature and altitude, respectively. These profiles show that distinct inversion layers repeatedly appeared below ~1 km and at 2–4 km. The altitude of the lower inversion layer, interpreted as the top of the mixed layer, exhibited significant day-to-day variations. In contrast, the altitude of the upper layer, interpreted as the top of the planetary boundary layer (PBL), changed much more slowly. The radiosonde data obtained in the local morning (2300 UT, 0830 LT) and the meteorological data observed from the G-II aircraft exhibit similar features (not shown). These structures are commonly seen in strong subsidence regions [*Stull*, 1999]. In this study the top of the PBL is determined by the first distinct increase of $d\theta/dz$ above 1.5 km. Steep gradients in CO and NO_y profiles were generally seen at the top of PBL [*Takegawa et al.*, 2001], as is seen in the RH profiles. In cases where the increase in $d\theta/dz$ was not distinct, the RH, CO, and NO_y profiles were also used to determine the PBL height.

[9] Altitude profiles of CO, NO_x, and NO_y observed over the Arnhem Land region during BIBLE-B are shown in Figure 5. All of the 10-s data are plotted except for the data with CO $\geq$ 800 ppbv (fresh plumes, section 5.1). The mixing ratios of CO, NO_x, and NO_y below ~3 km showed significant enhancements, while those above ~3 km were fairly constant. This indicates that the well-defined PBL was a strong barrier to the vertical transport of biomass burning emissions over Arnhem Land during BIBLE-B. It is likely that the easterly or southeasterly wind in the PBL was the only effective pathway for transport of biomass burning plumes from northern Australia. It can be seen from Figure 2 that the region of subsidence stretched as far as the southern part

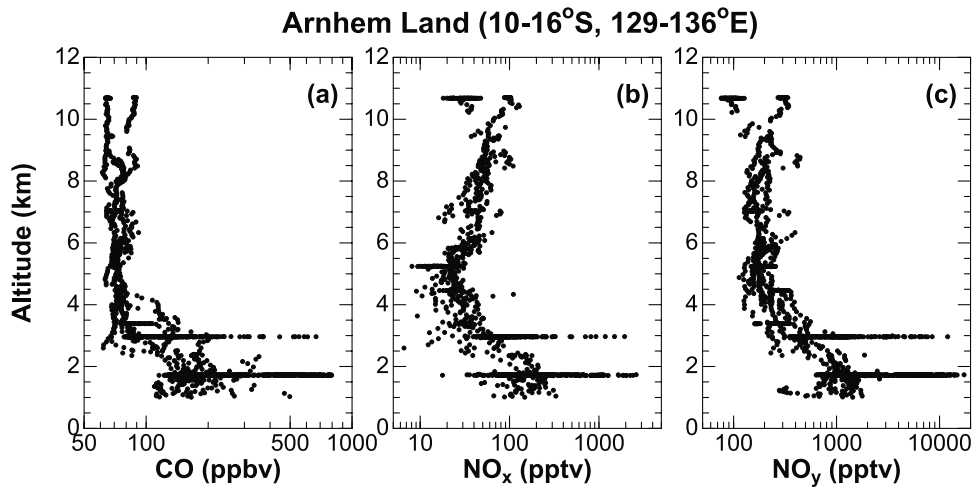

Figure 5. Altitude profiles of 10-s averaged mixing ratios of (a) CO, (b) NO_x, and (c) NO_y observed over the Arnhem Land region during BIBLE-B. Note that data with CO $\geq$ 800 ppbv (fresh plumes) were excluded.

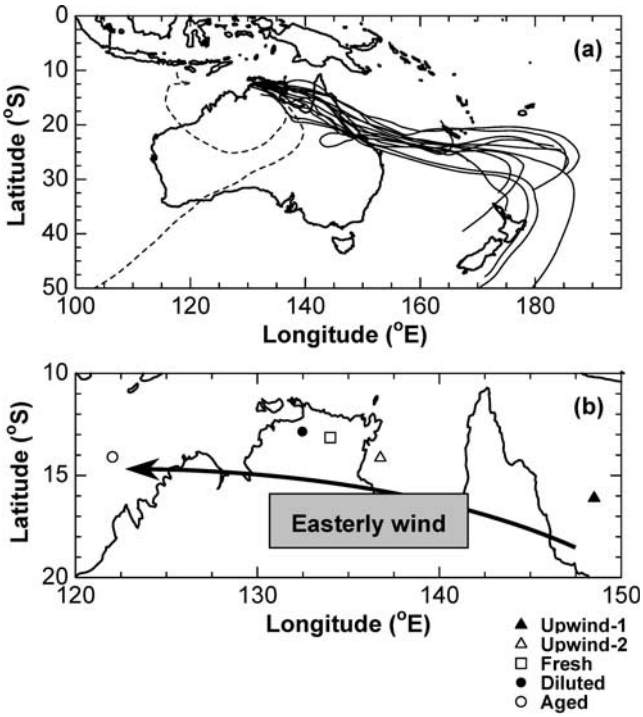

Figure 6. (a) Ten-day back trajectories for air masses observed in the PBL over Arnhem Land. Trajectories originating from the South Pacific Ocean are shown as solid lines, and others as dashed lines. These air masses passed over the Arnhem Land region (129°–136°E) in about 2 days. (b) Air mass classification in the PBL. The typical location where each air mass was sampled is shown on the map. The symbols for the different air mass classifications correspond to the same symbols shown in Figures 8–11.

of Indonesia (5°S, 110°E), suggesting that the clear contrast in the trace gas distributions between the boundary layer and free troposphere extended to this region. The major transport pathway of biomass burning plumes during BIBLE-B is likely representative of this season, considering the similarity in the meteorological conditions during BIBLE-B to those averaged for September of 1979–1995 (section 3).

5. Air Mass Classification

[10] Ten-day back trajectories were calculated for the sampled air masses using meteorological data, with a horizontal resolution of 2.5° in longitude and 2.5° in latitude, provided by the European Centre for Medium-Range Weather Forecasts (ECMWF) (http://www.ecmwf.int). Examples of trajectories for air masses observed in the PBL over Arnhem Land are shown in Figure 6a. About 90% of the trajectories originated from the South Pacific Ocean (5°–60°S, 160°E–160°W) and passed over the intensive biomass burning region prior to the measurements. In addition, almost all of the trajectories were confined to altitudes below 3 km for the previous 10 days. These air masses passed over the Arnhem Land region (129°–136°E) in about 2 days.

[11] The air masses sampled in the PBL were classified into five categories based on the air mass trajectories and CO mixing ratios (Figure 6b and Table 2). About 90% of the air samplings during BIBLE-B were made between late morning and afternoon (1100–1730 LT, solar zenith angle 20°–80°), when photochemical processes are considered to be active. Air masses sampled in the local morning (0900–1100 LT) were excluded from the present analysis. In addition, data obtained below 1 km over land, which were mostly sampled near airports, were excluded to avoid the influence of local pollution from Darwin city.

5.1. Fresh Plumes and Diluted Plumes

[12] Figure 7 shows time series plots of CO and NO_y mixing ratios obtained at 1.7 km over Arnhem Land on 4 September (flight 7). Large spikes of CO and NO_y were observed in intense smoke just above fires, coincident with the locations of hot spots shown in Figure 1. The width of each burning plume was 1–2 km, and the distance from one plume to another was approximately <100 km (at least one large hot spot in each 1° × 1° grid). The air masses observed in the PBL over Arnhem Land with CO $\geq$ 800 ppbv are referred to as fresh plumes, and those with CO < 800 ppbv are referred to as diluted plumes (Table 2 and Figure 6b). The criterion of CO = 800 ppbv was chosen rather arbitrarily. Air masses observed in the clouds at the top of the PBL (altitude 2.9 km) were excluded from the fresh and diluted plumes. The elapsed time since the recent injection of biomass burning emissions (elapsed time since emission) for the fresh plumes is estimated to be nearly zero because these plumes were sampled just above fires. The elapsed time since emission for the diluted plumes is estimated to be less than ~0.5 days, when the distribution of hot spots and horizontal eddy diffusion are taken into consideration [*Gifford*, 1982; *Mauzerall et al.*, 1998]. Because the fresh and diluted plumes were sampled during the local midday and afternoon, it is likely that these plumes

Table 2. Air Mass Classification During BIBLE-B

Air Mass	Upwind-1 Air	Upwind-2 Air	Fresh Plume	Diluted Plume	Aged Plume
Sampling Location	Cairns	Gulf of Carpentaria	Arnhem Land	Arnhem Land	Timor Sea
Sampling Latitude	16°–17°S	14°S	13°–14°S	10°–16°S	14°S
Sampling Longitude	146°–149°E	136.5°–137°E	131°–135°E	129°–136°E	122°–124°E
Sampling Altitude	1–3 km	1.7 km	1.7 km	1–3 km	0.7–2 km
CO Range	67–82 ppbv	84–99 ppbv	809–2734 ppbv	116–797 ppbv	147–237 ppbv
CO Median	77 ppbv	89 ppbv	980 ppbv	189 ppbv	189 ppbv
Number of Samples[a]	83	15	32	891	27
Time Since Emission[b]	–	–	~0	Less than ~ 0.5 days	2–3 days

[a]The number of 10-s averaged CO data.
[b]Elapsed time since the recent injection of biomass burning emissions (see text for details).

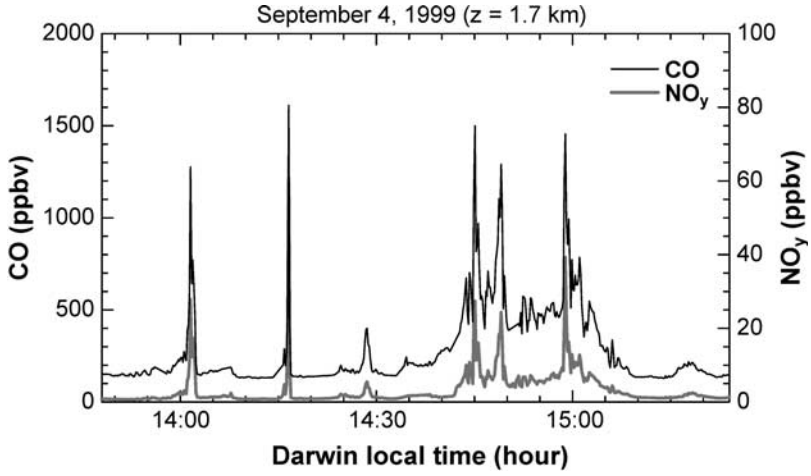

Figure 7. Time series of 10-s averaged CO (solid line) and NO_y (shaded line) mixing ratios obtained at 1.7 km over Arnhem Land on 4 September 1999.

had experienced mainly daytime conditions after the recent injection of biomass burning emissions. Therefore, the analysis of these plumes provides information on the photochemical and transport processes during the daytime.

5.2. Upwind Air

[13] In order to evaluate the impact of biomass burning emissions on trace gases over Arnhem Land, it is necessary to estimate their background mixing ratios in this region. The air masses upwind of the Arnhem Land region were sampled at 1–3 km near Cairns (16°–17°S, 146°–149°E) and also at 1.7 km over the Gulf of Carpentaria (13°S, 136.5°–137°E) (Table 2 and Figure 6b). These two air masses are referred to as upwind-1 air and upwind-2 air, respectively. The median CO mixing ratios in the upwind-1 and upwind-2 air were 77 and 89 ppbv, respectively. The slightly higher CO mixing ratios in the upwind-2 air were likely due to the effects of biomass burning over the Cape York Peninsula, because some of the trajectories passed over the sparse hot spots in this region (Figures 1 and 6a). These data are used for determining the background mixing ratios of trace gases (section 6.1).

5.3. Aged Plumes

[14] A flight over the Timor Sea (14°S, 122°–124°E), downwind of Arnhem Land under easterly flow conditions, was conducted at 0.5–13 km at 1100–1200 LT on 7 September 1999. A significant inversion layer was clearly identified at ~0.7 km over the Timor Sea, defining the top of the marine boundary layer (MBL). In addition, weak inversion layers were identified at ~2 km and at ~2.6 km. Steep gradients in CO and RH profiles can be seen around these inversions. Trajectories show that all of the air masses observed below 2 km over the Timor Sea had passed over the intensive biomass burning region of Arnhem Land 2–3 days prior to the measurements and were confined to altitudes below 3 km for a week, which is similar to the transport pattern shown in Figure 6a. Indeed, the CO mixing ratios between 0.7 and 2 km were significantly enhanced (CO = 150–240 ppbv). However, the CO mixing ratios in the MBL (<0.7 km) were comparable to those in the upwind air. One possible reason for the difference in the two regions, despite the similarity in the estimated air mass origins, is that the trajectories do not appropriately reproduce the transport patterns near the surface, or that biomass burning plumes were lifted up during their westward transport. The air masses sampled between 0.7 and 2 km over the Timor Sea are referred to as aged plumes (Table 2 and Figure 6b). The elapsed time since emission for the aged plumes is estimated to be 2–3 days, because the trajectories had passed over the Arnhem Land region 2–3 days prior to the measurements. Because the number of aged plume samples is limited (Table 2), the aged plume data may not represent the typical mixing ratios of trace gases in the boundary layer over the Timor Sea. However, in the correlation analysis discussed in section 6, the variability in the mixing ratios upon emission can be compensated for, as long as the emission ratios among trace gases are nearly constant.

6. Method of Analysis

6.1. Enhancements Above Background Levels

[15] The enhancement of a chemical species X (= CO, NO_x, NO_y, and NMHCs) above background in fresh, diluted, and aged plumes is defined as follows:

$$\Delta X = X - X_B, \tag{1}$$

where X is the mixing ratio of X in each plume and X_B is mixing ratio of X in the background air. The background mixing ratio is defined as follows

$$X_B = \left(X^{\mathrm{M}}_{\mathrm{up}-1} + X^{\mathrm{M}}_{\mathrm{up}-2}\right)/2, \tag{2}$$

$$\text{Uncertainty of } X_B = \pm\left(X^{\mathrm{M}}_{\mathrm{up}-2} - X^{\mathrm{M}}_{\mathrm{up}-1}\right)/2, \tag{3}$$

where $X^{\mathrm{M}}_{\mathrm{up}-1}$ and $X^{\mathrm{M}}_{\mathrm{up}-2}$ are the median mixing ratios in the upwind-1 and upwind-2 air, respectively. Hereafter, the superscript "M" denotes the median. We use median for consistency with the other classes (fresh, diluted, and aged plumes), though the medians are almost the same as the

Table 3. Background Mixing Ratios Over Arnhem Land[a]

Species	Background	Uncertainty
CO	83	6
Ethane (C_2H_6)	320	9
Ethyne (C_2H_2)	90	18
Propane (C_3H_8)	20	1
n-Butane (*n*-C_4H_{10})	4	<1
Toluene (C_7H_8)	–	–
Ethene (C_2H_4)	19	5
Propene (C_3H_6)	–	–
1-Butene (1-C_4H_8)	–	–
NO_x	17	6
NO_y	230	130

[a]Average of medians for upwind-1 and upwind-2 air. Units are ppbv for CO and pptv for others. The symbol "-" means lower than the limit of detection (3 pptv for NMHCs).

means for the upwind-1 and upwind-2 air. The uncertainty is defined as a difference between X^{M}_{up-1} and X^{M}_{up-2}. The X_B values and their uncertainties are summarized in Table 3. For the trace gases that are primarily emitted from biomass burning (CO, NO_x, NO_y, and NMHCs), the background mixing ratios and their uncertainties are much smaller than the enhancements in the fresh and diluted plumes. As the plumes travel downwind, they are diluted through the entrainment of air masses in the free troposphere (3–5 km). In terms of the effect on the ΔX values, the mixing with free tropospheric air is equivalent to the mixing with the background air because the mixing ratios of CO, NO_x, NO_y, and NMHCs at 3–5 km are similar to those in the background air (Table 3 and Figure 5).

6.2. $\Delta Y/\Delta X$ Ratios

[16] If a particular pair of chemical species X and Y is considered, the $\Delta Y/\Delta X$ ratio is useful for characterizing the photochemical and dilution processes in biomass burning plumes. Here the $\Delta Y/\Delta X$ ratio is given as the gradient of a straight line joining the data point to the background value (equation (1)). The data, consisting of biomass burning plumes up to 3 days old, are interpreted using the following assumptions: (1) biomass burning is the dominant source of X and Y, (2) the emission ratio of Y to X from biomass burning is constant, and (3) the background mixing ratios of X and Y are constant with time. In our discussion, the species with diurnally averaged photochemical lifetimes of more than 3 times longer than the time since emission for aged plumes (2–3 days) are referred to as long-lived species and the others as short-lived species. It is instructive to consider three special cases, as summarized below. The details of the formulations are given in Appendix A.

6.2.1. Case 1: X and Y are Both Long-Lived Species

[17] The $\Delta Y/\Delta X$ ratio in the plumes should not change with air mass aging because dilution is a linear process. With the emission ratio assumed to be constant, the correlation plot of Y versus X follows the line defined below:

$$(Y - Y_B)/(X - X_B) = (\Delta Y/\Delta X)^{M}_{fresh}, \quad (4)$$

where $(\Delta Y/\Delta X)^{M}_{fresh}$ is the median of the $\Delta Y/\Delta X$ ratios in the fresh plumes and is equal to the emission ratio of Y to X. The line defined by equation (4) has a gradient equal to $(\Delta Y/\Delta X)^{M}_{fresh}$ and passes through the background point (X_B, Y_B). Hereafter this line is referred to as the Y-X dilution line.

6.2.2. Case 2: X is a Long-Lived Species and Y is a Short-Lived Species

[18] The $\Delta Y/\Delta X$ ratios in the diluted and aged plumes should decrease with air mass aging due to the chemical loss of Y. The data points showing the correlations of Y versus X (with X plotted on the horizontal axis) lie below the Y-X dilution line. The $\Delta Y/\Delta X$ ratios normalized by the emission ratio give the fraction of Y molecules emitted from biomass burning remaining in the observed air masses. This method was utilized to estimate the removal of NO_y in previous studies [e.g., *Stohl et al.*, 2002] and is also utilized to estimate the removal of NO_y in this study (section 7.3).

6.2.3. Case 3: X and Y are Both Short-Lived Species

[19] The $\Delta Y/\Delta X$ ratios should decrease or increase with air mass aging, depending on which species has the shorter photochemical lifetime. If the lifetimes of X and Y are identical, the $\Delta Y/\Delta X$ ratios should not change with air mass aging and follow the dilution line. The photochemical lifetime of NO_x is estimated based on this consideration (section 7.2).

7. Results and Discussion

[20] The photochemical lifetimes of NMHCs under BIBLE-B conditions were estimated considering the chemical losses by hydroxyl radical (OH) and are summarized in Table 4. The OH concentrations were calculated by the AER photochemical point model, while the kinetic parameters listed by *Gery et al.* [1989], *Atkinson et al.* [1997], and *Calvert et al.* [2000] were used for calculating the rate coefficients of OH reactions. As discussed in section 5.1, the diluted plumes were sampled between late morning and afternoon, and these plumes had experienced mainly daytime conditions since emission. Therefore, the median OH concentration in the diluted plumes (daytime) should be used in estimating the photochemical lifetimes of NMHCs in these plumes rather than the diurnally averaged OH concentration. The median value of the calculated OH concentrations in the diluted plumes is 5.5×10^6 cm^{-3},

Table 4. Photochemical Lifetimes of CO and NMHCs Under Conditions Appropriate for BIBLE-B[a]

	Lifetime, days	
Species	Diluted Plumes[b]	Diurnal Average[c]
CO	9.4	27
C_2H_6	10	30
C_2H_2	3.1	8.9
C_3H_8	2.1	6.1
n-C_4H_{10}	0.88	2.6
C_7H_8	0.34	0.98
C_2H_4	0.26	0.77
C_3H_6	0.07	0.21
1-C_4H_8	0.06	0.18

[a]Photochemical lifetimes against oxidation by OH at median pressure (823 hPa) and temperature (285 K) in the diluted plumes. The OH concentrations were calculated using the AER box model.

[b]Median value of OH concentration in the diluted plumes (5.5×10^6 cm^{-3}) is used because these plumes had experienced mainly daytime conditions since emission (section 5.1).

[c]Diurnally averaged OH concentration in the diluted plumes (1.9×10^6 cm^{-3}) is used.

Table 5. Median Values of ΔY/ΔCO Ratios in Each Air Mass Class[a]

Y	Fresh Plumes	Diluted Plumes	Aged Plumes
C_2H_6	2.6 (+0.3/−0.1)	2.6 (+0.3/−0.3)	2.1 (+0.1/−0.1)
C_2H_2	2.9 (+0.2/−0.1)	3.1 (+0.3/−0.3)	2.9 (+0.1/−0.2)
C_3H_8	0.55 (+0.07/−0.01)	0.5 (+0.1/−0.1)	0.24 (+0.04/−0.05)
n-C_4H_{10}	0.11 (+0.01/−0.01)	0.07 (+0.03/−0.02)	0.02 (+0.01/−0.01)
C_7H_8	0.29 (+0.02/−0.02)	0.22 (+0.07/−0.08)	0.04 (+0.01/−0.01)
C_2H_4	7.0 (+0.2/−0.2)	3 (+2/−2)	0.20 (+0.02/−0.02)
C_3H_6	1.8 (+0.1/−0.2)	0.4 (+0.6/−0.2)	0.01 (+0.02/−0.01)
1-C_4H_8	0.25 (+0.01/−0.02)	0.0 (+0.1/−0.0)	–
NO_x	N/A	1.7 (+0.8/−0.5)	0.7 (+0.1/−0.2)
NO_y	18 (+2/−2)	14 (+4/−3)	7.0 (+0.5/−1.1)

[a]Units are pptv/ppbv. Values in parentheses denote the central 67% ranges. The symbol "–" means that mixing ratios are lower than the limit of detection. The symbol "N/A" means that the data are not available.

which agrees well with typical midday OH concentrations in the boundary layer observed during the Pacific Exploratory Mission (PEM) - Tropics A ($6–8 \times 10^6$ cm^{-3}) [*Mauldin et al.*, 1999]. The median $\Delta Y/\Delta CO$ ratios in each air mass class, $(\Delta Y/\Delta CO)^M$, are summarized in Table 5, where Y denotes NMHCs, NO_x, and NO_y. Because the O_3 data in the fresh plumes and some of the O_3 data at CO > 400 ppbv in the diluted plumes were not obtained, the corresponding NO_2 values, and therefore NO_x values, were not available.

7.1. Correlations of NMHCs and CO

[21] In this section, correlations of NMHCs with CO (or other NMHCs) are used to demonstrate that the method of the analysis described in section 6 is suitable for interpreting the observed behaviors of trace gases in the PBL. Correlations of ethyne (C_2H_2) and ethene (C_2H_4) with CO in the background air, fresh plumes, diluted plumes, and aged plumes are shown in Figures 8a and 8b, and those of 1-butene (1-C_4H_8) with propene (C_3H_6) are shown in Figure 8c. The solid line is the dilution line with a gradient equal to the median $\Delta Y/\Delta X$ ratio in the fresh plumes (Table 5). The dashed line has a gradient equal to the median $\Delta Y/\Delta X$ ratio in the aged plumes.

7.1.1. Case 1: Long-Lived (C_2H_2) Versus Long-Lived (CO) Species

[22] The $\Delta C_2H_2/\Delta CO$ ratios in the diluted and aged plumes are similar to those in the fresh plumes (Table 5), and the correlations of C_2H_2 with CO in the diluted and aged plumes approximately follow the dilution line (Figure 8a). Correlation of C_2H_6 with CO shows similar behavior to that of C_2H_2 (Table 5). The data samples were obtained from numerous plumes. The fact that the data from these plumes fall on the same dilution line indicates that biomass burning was the dominant source of CO, C_2H_6, and C_2H_2 in this region, and that the emission ratios of C_2H_6 and C_2H_2 to CO were very uniform. Indeed, poor correlation of tetrachloroethene (C_2Cl_4, an urban pollution tracer) with CO was found in the fresh, diluted, and aged plumes, suggesting that industrial pollution made a negligible contribution to the trace gas source in this region. It is known that both CO and NMHCs are emitted predominantly in the smoldering combustion stage of biomass fires [e.g., *Crutzen and Andreae*, 1990]. The uniformity of emission ratios of C_2H_6 and C_2H_2 to CO in the Arnhem Land region can be attributed to the homogeneity of vegetation in this region [*Russell-Smith et al.*, 2003]. Analogous to C_2H_6 and C_2H_2, it is likely that the emission ratios of NMHCs to CO were also uniform for other NMHCs given in Table 5. Indeed, the ΔNMHC/ΔCO ratios in the fresh plumes were nearly constant for these NMHCs (Table 5).

7.1.2. Case 2: Short-Lived (C_2H_4) Versus Long-Lived (CO) Species

[23] The $\Delta C_2H_4/\Delta CO$ ratios in the diluted and aged plumes are systematically smaller than those in the fresh plumes (Table 5), and the correlations of C_2H_4 with CO in the diluted and aged plumes lie below the dilution line

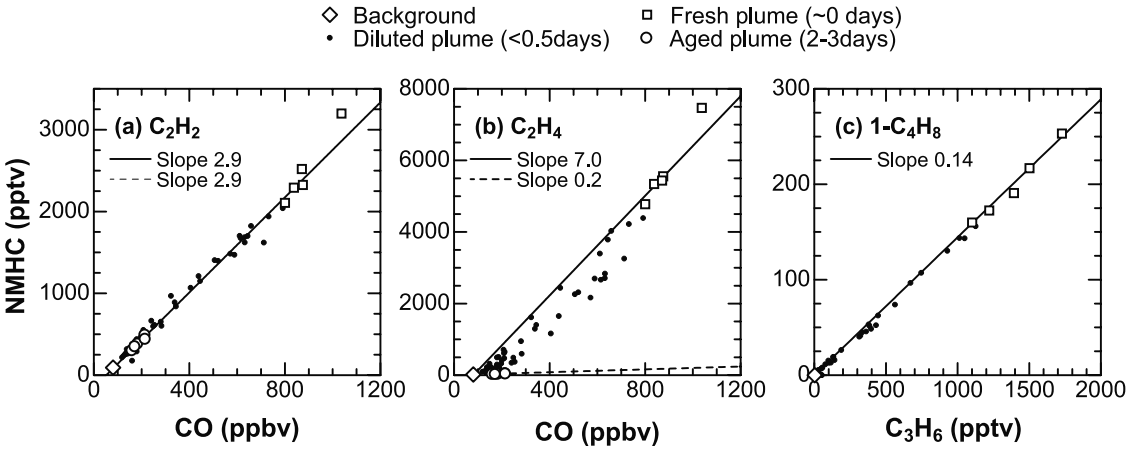

Figure 8. Correlations of (a) ethyne (C_2H_2) and (b) ethene (C_2H_4) versus CO in the background air (diamonds), fresh plumes (squares), diluted plumes (solid circles), and aged plumes (open circles). The solid line represents the NMHC-CO dilution line defined by equation (4). The dashed line has a slope equal to the median ΔNMHC/ΔCO ratio in the aged plumes and passes through the background point. Note that the solid line overlaps the dashed line in Figure 8a. (c) Same as Figure 8a, but for the correlation of 1-butene (1-C_4H_8) with propene (C_3H_6). The background mixing ratios of C_3H_6 and 1-C_4H_8 are assumed to be zero because they are below the detection limit of 3 pptv.

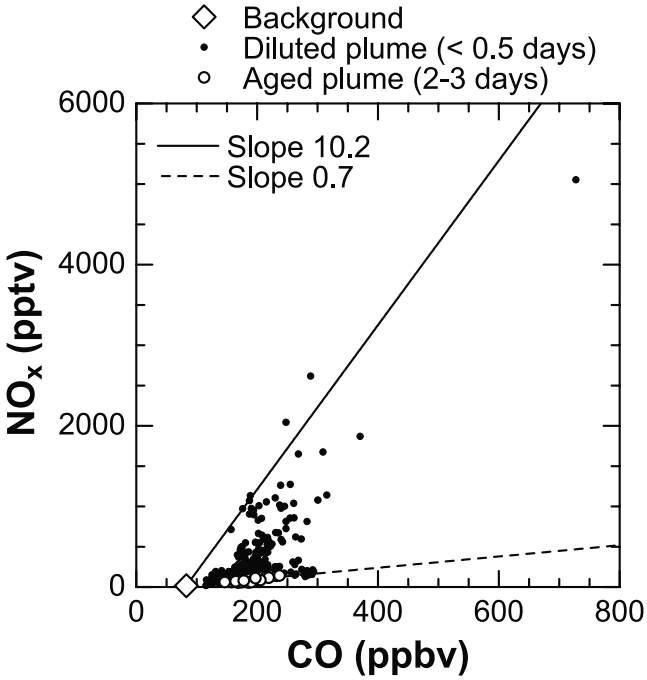

Figure 9. Correlation plots of NO_x with CO in the background air (diamond), diluted plumes (solid circles), and aged plumes (open circles). The solid line is the NO_x-CO approximate dilution line (see text for details). The average of the $\Delta NO_x/\Delta CO$ ratios at the highest two NO_x mixing ratios (NO_x = 2620 and 5050 pptv) is used to determine the slope of this line. The dashed line has a gradient equal to the median $\Delta NO_x/\Delta CO$ ratio in the aged plumes and passes through the background point.

(Figure 8b). Other short-lived NMHCs, such as *n*-butane (*n*-C_4H_{10}), toluene (C_7H_8), and propene (C_3H_6) show similar behavior (Table 5). It should be noted that the decreasing rate of the $(\Delta NMHC/\Delta CO)^M$ values during air mass aging (from fresh to aged plumes) was consistently faster for shorter-lived NMHC (Table 5).

7.1.3. Case 3: Short-Lived (1-C_4H_8) Versus Short-Lived (C_3H_6) Species

[24] The photochemical lifetimes of 1-C_4H_8 and C_3H_6 are nearly the same in the diluted plumes (Table 4). Indeed, the correlation of 1-C_4H_8 with C_3H_6 in these plumes approximately follows the dilution line (Figure 8c), as expected.

7.2. NO_x Oxidation in Diluted and Aged Plumes

[25] Correlations of NO_x with CO in the background air, diluted plumes, and aged plumes are shown in Figure 9. Although the NO_x data in the fresh plumes were not available, the NO_x-CO emission ratio in this region can be regarded as nearly constant because the NO_y-CO emission ratio estimated from the $\Delta NO_y/\Delta CO$ ratios in the fresh plumes was found to be very uniform (Table 5). Details of the NO_y-CO emission ratio are discussed in section 7.3. Instead of using the dilution line defined by equation (4), we use the approximate dilution line that has a slope equal to the average of the $\Delta NO_x/\Delta CO$ ratios at the highest two NO_x mixing ratios (NO_x = 2620 and 5050 pptv). This slope is somewhat lower than the NO_y-CO emission ratio (Table 5), suggesting slight oxidation of NO_x even at these high NO_x levels. Almost all the data points lie below the approximate dilution line, indicating that further oxidation of NO_x proceeded in the diluted plumes. It is noted that there are no data points with high NO_x mixing ratios near the CO background level, suggesting that biogenic emissions from savanna soils [*Parsons et al.*, 1996] had a minor contribution to NO_x sources in this region.

[26] The photochemical lifetime of NO_x in the diluted plumes can be estimated using the correlations of NO_x with short-lived NMHCs with known photochemical lifetimes. Figure 10 shows the correlations of NO_x with C_7H_8, C_2H_4, and C_3H_6 in the diluted plumes. The approximate dilution line for the NO_x-NMHC correlation has been determined in the same way as for the NO_x-CO correlation and is shown in Figure 10. As discussed in sections 6.2 and 7.1, the $\Delta Y/\Delta X$ ratios do not change with air mass aging if the photochemical lifetimes of X and Y are identical. The correlations of NO_x with C_7H_8 and C_2H_4 mostly lie below the approximate dilution line, while that of NO_x with C_3H_6 mostly lies

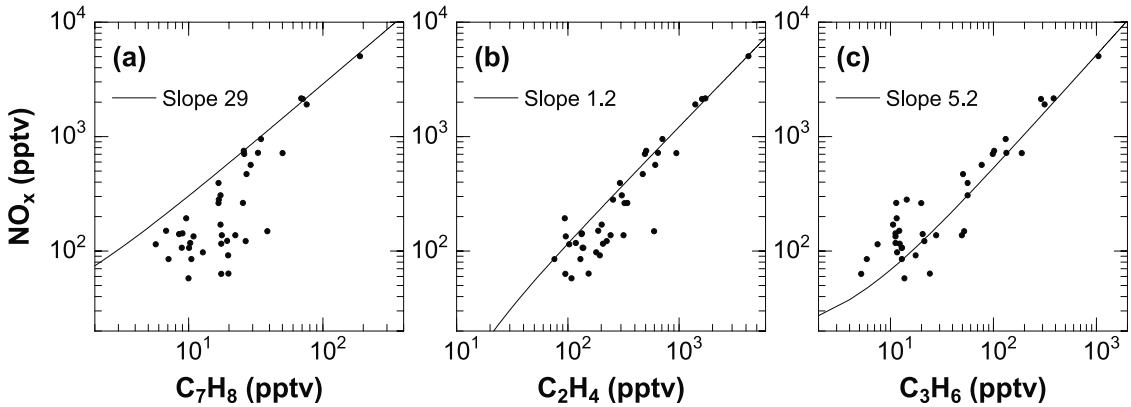

Figure 10. Correlations of NO_x with (a) toluene (C_7H_8), (b) ethene (C_2H_4), and (c) propene (C_3H_6) in the diluted plumes. The lines represent the approximate dilution lines. The average of the $\Delta NO_x/\Delta NMHC$ ratios at the highest two NO_x mixing ratios (NO_x = 2150 and 5020 pptv) is used to determine the slope of these lines. The background mixing ratio of C_7H_8 is assumed to be zero. Note that the straight line appears curved in the log-log plot.

above the line. This result demonstrates that the photochemical lifetime of NO_x in the diluted plumes was longer than that of C_3H_6 (~0.1 days) and shorter than that of C_2H_4 (~0.3 days).

[27] The NO_x lifetime against the reaction of NO_2 + OH to form HNO_3 is estimated to be 0.33 (+0.04/−0.03) days for the diluted plumes:

$$\left\{(NO_2/NO_x)^M\, k_{NO2+OH}[OH]\right\}^{-1} = 0.33(+0.04/-0.03)\text{days} \quad (5)$$

$(NO_2/NO_x)^M$ = 0.67 (+0.07/−0.03) is the median NO_2/NO_x ratio (± central 67% range) in the diluted plumes. k_{NO2+OH} is the reaction rate coefficient of NO_2 + OH reaction [*Sander et al.*, 2000]. The median values of pressure and temperature in the diluted plumes were used for calculating k_{NO2+OH}. The uncertainties in the reaction rate coefficients and OH concentration are not taken into consideration. These results show that the reaction NO_2 + OH (lifetime 0.33 days) explains about half of the net loss of NO_x (lifetime 0.1–0.3 days) in the diluted plumes.

[28] Conversion of HNO_3 to NO_x, if it occurs at a substantial rate, will influence the net NO_x oxidation rate. The time constant for gas-phase conversion of HNO_3 to NO_x at 0–4 km over the South Atlantic Basin during TRACE-A was estimated to be much longer than a day [*Jacob et al.*, 1996]. *Saathoff et al.* [2001] reported that the heterogeneous reaction of HNO_3 on soot aerosol to form NO_x [*Lary et al.*, 1997] was negligible under the conditions where soot concentrations were lower than 200 μg m^{-3}, based on laboratory experiments. According to this study, the effect of this heterogeneous process will be negligibly small in the diluted plumes because the soot concentrations were typically lower than 30 μg m^{-3} [*Liley et al.*, 2002]. The rest of the NO_x removal is probably explained by the formation of organic nitrates including PAN. Indeed, rapid formation of PAN was observed in 0.5-day-old biomass burning plumes at 0–4 km over the Amazon or southern Africa during TRACE-A [*Mauzerall et al.*, 1998].

7.3. NO_y Removal in Diluted and Aged Plumes

[29] Correlations of NO_y with CO in the background air, fresh plumes, diluted plumes, and aged plumes are shown in Figure 11. The NO_y-CO dilution line defined by equation (4) and the line with a slope of $(\Delta NO_y/\Delta CO)^M$ for the aged plumes are also shown in the plot. Except for a few outlying data points above the dilution line, the $\Delta NO_y/\Delta CO$ ratios in the fresh plumes are found to be very uniform. This indicates that the emission ratio of NO_y to CO from biomass burning can be regarded as nearly constant in the Arnhem Land region. The uniformity of emission ratio of NO_y to CO can be attributed to the uniformity of combustion efficiency in this region [*Shirai et al.*, 2003] as well as the homogeneity of vegetation [*Russell-Smith et al.*, 2003]. The NO_y to CO emission ratio obtained here (18 ± 2 pptv/ppbv) is comparable to the NO_x to CO emission ratio previously observed in Australian savanna fires. *Hurst et al.* [1994] reported NO_x to CO emission ratios of 8–56 pptv/ppbv (average 23 ± 10 pptv/ppbv). *Sawa et al.* [1999] reported an average NO_x to CO emission ratio of 11 ± 1 pptv/ppbv in Australian savanna fires.

[30] Most of the data points in the diluted and aged plumes lie below the dilution line (Figure 11). Decreases

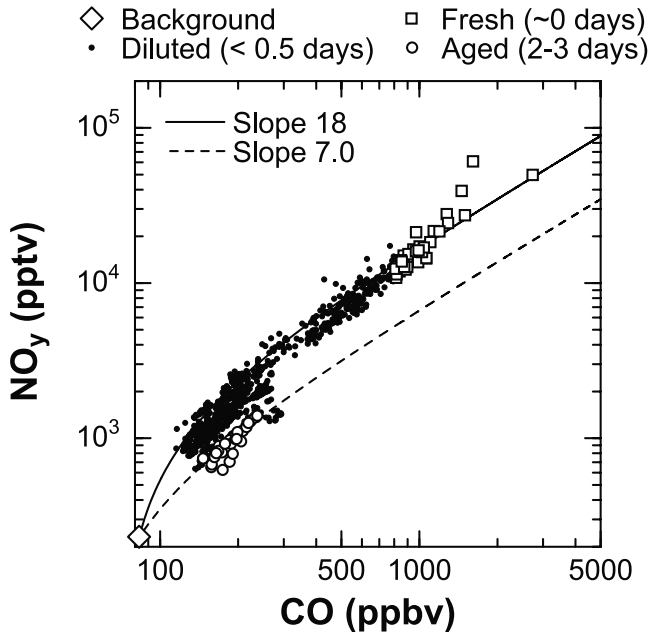

Figure 11. Same as Figure 8, but for the NO_y-CO correlation.

in NO_y relative to CO can be seen particularly at lower CO concentrations in the diluted plumes and at all concentrations in the aged plumes. Because there was little precipitation over northern Australia during BIBLE-B, the major sink of NO_y is considered to be the dry deposition of HNO_3 or aerosol nitrate. The $(\Delta NO_y/\Delta CO)^M$ values in the diluted (<0.5 days) and aged plumes (2–3 days) are ~80% and ~40% of the emission ratio of NO_y to CO, respectively, leading to an estimate that ~20% (~60%) of the NO_y molecules emitted from biomass burning were removed from the air masses within 0.5 days (2–3 days) by dry deposition. Considering that biomass burning plumes were mostly confined within the PBL over northern Australia and the Timor Sea (sections 4 and 5), it is likely that only a small fraction of NO_y was exported to the free troposphere during BIBLE-B.

[31] We now estimate the rate of NO_y removal caused by HNO_3 dry deposition using a simple model. Here we consider a vertical column in the PBL over Arnhem Land and assume that the NO_y number densities in this column are uniform. The NO_y number density at time t in this vertical column, $C(t)$, can be approximated as follows:

$$h_{BL}\, dC(t)/dt = -v_d R_{HNO3} C(t), \quad (6)$$

where h_{BL} is the typical PBL height (=2.5 km), v_d is deposition velocity for HNO_3, and R_{HNO3} is the HNO_3/NO_y ratio in the diluted plumes. Assuming that these three parameters are constant with time, we obtain a simple solution:

$$C(t) = C(0)\exp(-v_d R_{HNO3} t/h_{BL}). \quad (7)$$

The HNO_3 deposition velocity largely depends on the surface conditions and ranges from 1 to 5 cm s^{-1} [*Lovett*, 1994]. We assume it to be 3 cm s^{-1}. The median value of

($NO_y - NO_x$)/NO_y ratios in the diluted plumes is 0.8. We vary the R_{HNO3} value from 0.4 to 0.8 in equation (7), so as to estimate possible errors due to the assumption that R_{HNO3} is constant with time. The $C(t)/C(0)$ ratio is calculated to be 0.7–0.8 for t = 0.5 days and 0.1–0.3 for t = 3 days, for the range of R_{HNO3} considered. Despite the large uncertainties in the above estimates, the observed decrease in NO_y in the diluted and aged plumes can be explained approximately by HNO_3 dry deposition. The effect of aerosol dry deposition cannot be evaluated because of the lack of aerosol composition data.

[32] The removal of NO_y in the boundary layer has also been reported in earlier studies. *Liang et al.* [1998] reported that 66–74% of NO_y molecules emitted from the United States could be removed by dry/wet deposition in the boundary layer, based on three-dimensional model simulations. *Stohl et al.* [2002] have also reported an effective mean NO_y lifetime of ~1.7 days in the North Atlantic boundary layer, based on aircraft data obtained during the North Atlantic Regional Experiment in spring 1996 and fall 1997 (NARE 96, 97). They found that 33–91% of the surface emissions of NO_y were removed within the boundary layer or during transport from it, under a variety of meteorological conditions that led to transport of air from the boundary layer to the free troposphere.

[33] We have estimated the removal rate of NO_y under the conditions appropriate for the BIBLE-B measurements. This estimate is not necessarily applicable to other regions/seasons, because various factors such as surface conditions (deposition velocity), boundary layer height (time constant for vertical mixing), and precipitation (wet deposition) control the NO_y removal rate. However, a common feature obtained in this study and the earlier studies is that a large fraction of NO_y emitted from surface sources is lost in the PBL due to dry/wet deposition of HNO_3 or aerosol nitrate. Such an estimate is important for evaluating the contributions of surface emissions to the NO_y budget in the free troposphere, where horizontal transport is more effective due to greater wind speeds. It is also important for assessing the effects of acid deposition on the surface environment.

7.4. Decrease in NO_x and NO_y With Air Mass Aging

[34] Here we use the relative age to qualitatively investigate the decreases in NO_x and NO_y in the diluted plumes. Details of the derivation of the relative age are given in Appendix A. The relative age is defined using a ratio of a short-lived species Y to a long-lived species X

$$\text{Relative age} = \ln\left(\frac{(\Delta Y/\Delta X)^{M}_{\text{fresh}}}{\Delta Y/\Delta X}\right). \quad (8)$$

We use X = CO and Y = C_2H_4 because C_2H_4 has a large emission ratio relative to CO, and the photochemical lifetime of 0.26 days is appropriate for resolving the history in the diluted plumes that are <0.5 days old. Because the relative age is zero for the fresh plumes and increases with time, it can be used as a qualitative indicator of air mass aging. The data near the background levels (CO < 120 ppbv and C_2H_4 < 60 pptv) were excluded because the $\Delta C_2H_4/\Delta CO$ ratios for these data have much larger uncertainties (see Table 3).

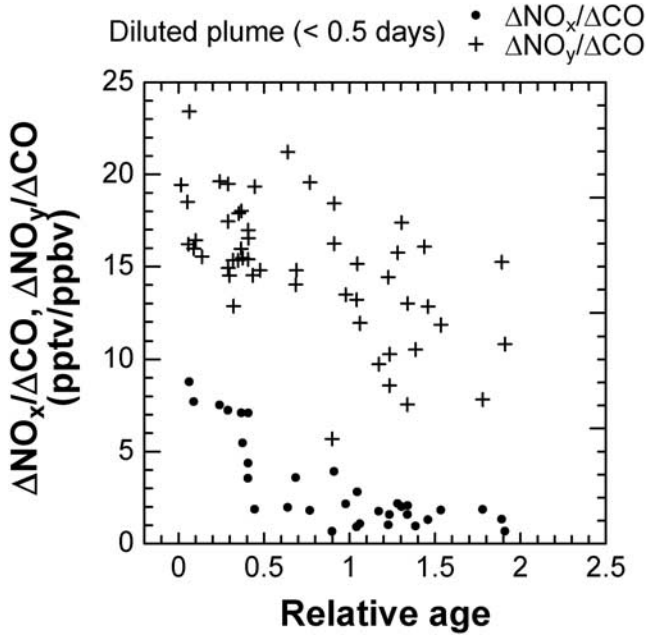

Figure 12. $\Delta NO_x/\Delta CO$ (dots) and $\Delta NO_y/\Delta CO$ (crosses) ratios as a function of relative age in the diluted plumes. The relative age is defined using the $\Delta C_2H_4/\Delta CO$ ratios. See Appendix A for details.

[35] The $\Delta NO_x/\Delta CO$ and $\Delta NO_y/\Delta CO$ ratios in the diluted plumes are plotted as a function of relative age in Figure 12. It clearly shows that both $\Delta NO_x/\Delta CO$ and $\Delta NO_y/\Delta CO$ ratios systematically decrease with air mass aging. The decay rate of the $\Delta NO_y/\Delta CO$ ratio is nearly zero at the initial stage (relative age less than ~1), and increases with air mass aging (relative age greater than ~1). This feature may be interpreted in terms of changes in NO_y partitioning. Most of the NO_y compounds should be in the form of NO_x in the fresh plumes. First, NO_x is oxidized to other NO_y compounds (HNO_3, PAN, and aerosol nitrate) without leading to a net loss of NO_y. The loss of NO_y is accelerated with the increase in the HNO_3/NO_y or aerosol nitrate/NO_y ratios, because the removal of NO_y is most effective through the deposition of these species.

8. Conclusions

[36] In this paper we studied the removal processes of NO_x and NO_y in biomass burning plumes in the PBL over northern Australia, using the data set obtained during the BIBLE-B aircraft measurement campaign in August–September 1999. The biomass burning emissions in this region were mostly confined to the PBL (below ~3 km) by strong subsidence in the free troposphere. The easterly or southeasterly wind in the PBL was the only effective pathway to transport the biomass burning plumes from northern Australia during this period. This simple horizontal transport pattern enabled us to classify the observed air masses according to their photochemical history: upwind-1 air (CO 70–80 ppbv), upwind-2 air (80–100 ppbv), fresh plumes (800–2700 ppbv), diluted plumes (120–800 ppbv), and aged plumes (150–240 ppbv). The upwind air was used to determine the background mixing ratios of trace

gases over the Arnhem Land region. The fresh plume data were used to determine the emission ratios among trace gases from biomass burning in this region. The elapsed time since the recent injection of biomass burning emissions into the plumes was estimated to be less than ~0.5 days and 2–3 days for the diluted and aged plumes, respectively.

[37] In order to describe the photochemical history of trace gases in the plumes, we analyzed the changes in the $\Delta Y/\Delta X$ ratios (ΔX is the enhancement of species X above the background) in the fresh, diluted, and aged plumes. First, we examined the correlations of NMHCs with CO (or other NMHCs) for various NMHCs with known photochemical lifetimes and showed that the method of analysis is suitable for interpreting the observed behaviors of trace gases under BIBLE-B conditions.

[38] Second, we examined the changes in the $\Delta NO_x/\Delta CO$ and $\Delta NO_x/\Delta NMHC$ ratios to investigate the removal process of NO_x. A systematic decrease in the $\Delta NO_x/\Delta CO$ ratio was found both in the diluted and aged plumes, indicating the chemical loss of NO_x in these plumes. The photochemical lifetime of NO_x in the diluted plumes (daytime) was estimated using the $\Delta NO_x/\Delta C_2H_4$ and $\Delta NO_x/\Delta C_3H_6$ ratios. The $\Delta NO_x/\Delta C_2H_4$ ratios in the diluted plumes decreased with air mass aging, while the $\Delta NO_x/\Delta C_3H_6$ ratios increased, demonstrating that the photochemical lifetime of NO_x in the diluted plumes was longer than that of C_3H_6 (~0.1 days) and shorter than that of C_2H_4 (~0.3 days). The net loss of NO_x in these plumes is probably explained by the conversions of NO_x to HNO_3, PAN, and other organic nitrates.

[39] Finally, we examined the changes in the $\Delta NO_y/\Delta CO$ ratios to investigate the removal process of NO_y. A systematic decrease in the $\Delta NO_y/\Delta CO$ ratios was found in the diluted and aged plumes, indicating the loss of NO_y in these plumes. By comparing the median $\Delta NO_y/\Delta CO$ ratio in the diluted and aged plumes to that in the fresh plumes, it was estimated that ~60% of the NO_y molecules were removed from the air masses within 2–3 days. This result was consistent with the dry deposition of HNO_3 in the plumes. Because the well-defined PBL was a strong barrier to the vertical transport of biomass burning emissions, the results obtained in this study suggest that only a small fraction of NO_y emitted from biomass burning was exported to the free troposphere during the BIBLE-B period.

Appendix A: Interpretation of $\Delta Y/\Delta X$ Ratio

A.1. Single-Puff Injection

[40] We follow the approach introduced by *McKeen et al.* [1996] to describe the mixing ratio of species X (= CO, NO_x, NO_y, NMHCs, ...) in an air mass that experienced a puff emission at time $t = 0$ (resulting in a initial mixing ratio of X_0) and continues to mix with the background air. The mixing ratio of a species X is given by the following equation.

$$\frac{dX}{dt} = -L_X X - K(X - X_B), \tag{A1}$$

where L_X is the photochemical loss rate of X, X_B is the mixing ratio of X in the background air, and K is a mixing coefficient with background air. Assuming that L_X and K are constants in time, we obtain the analytical solution

$$X = \frac{K}{L_X + K} X_B + \left(X_0 - \frac{K}{L_X + K} X_B \right) e^{-(L_X + K)t}. \tag{A2}$$

If X is a long-lived species ($L_X \sim 0$), equation (A2) can be approximated as

$$X = (X_0 - X_B)e^{-Kt} + X_B \text{ i.e., } \Delta X = \Delta X_0 e^{-Kt}, \tag{A3}$$

where $\Delta X = X - X_B$ is the enhancement of X in each air mass and $\Delta X_0 = X_0 - X_B$ is the enhancement of X upon emission. If X is a short-lived species with negligible background ($X_B \sim 0$, $\Delta X = X - X_B \sim X$), equation (A2) can be approximated as

$$X = X_0 e^{-(L_X + K)t} \text{ i.e., } \Delta X = \Delta X_0 e^{-(L_X + K)t}. \tag{A4}$$

As readily seen from equations (A3) and (A4), we can compensate for the effect of dilution (K) by taking a ratio of two species in case of a single-puff injection.

A.2. Multiple Injections

[41] In this study the mixing ratio of X in an air mass is affected by multiple injections of biomass burning emissions as the air mass passes over hot spots. If X is a long-lived species, we assume that ΔX can be parameterized as

$$\Delta X = \sum_i \Delta X_i^0 e^{-Kt_i} = \Delta X_{\text{total}} \sum_i \alpha_i e^{-Kt_i} \tag{A5}$$

from equation (A3), where ΔX_i^0 is the initial enhancement of X for i-th injection ($i = 1, 2, \ldots, n$), t_i is the elapsed time since the i-th injection, $\Delta X_{\text{total}} = \sum_i \Delta X_i^0$ is the total amount injected, and $\alpha_i = \Delta X_i^0 / \Delta X_{\text{total}}$ is the relative contribution of the i-th injection ($\sum_i \alpha_i = 1$). If X is a short-lived species, we assume that ΔX can be parameterized as

$$\Delta X = \sum_i \Delta X_i^0 e^{-(L_X + K)t_i} = \Delta X_{\text{total}} \sum_i \alpha_i e^{-(L_X + K)t_i} \tag{A6}$$

from equation (A4). The same α_i can be used for different species as long as the emission ratios among species are the same for each injection. We consider two chemical species X and Y, and examine three special cases.

A.2.1. Case 1: X and Y Are Long-Lived Species

$$\frac{\Delta Y}{\Delta X} = \frac{\Delta Y_{\text{total}}}{\Delta X_{\text{total}}} \frac{\sum_i \alpha_i e^{-Kt_i}}{\sum_i \alpha_i e^{-Kt_i}} = \frac{\Delta Y_{\text{total}}}{\Delta X_{\text{total}}} = E_{Y-X}, \tag{A7}$$

where $E_{Y-X} = \Delta Y_{\text{total}} / \Delta X_{\text{total}}$ is the emission ratio of Y to X that are determined using the fresh plume data. Equation (A7) shows that the $\Delta Y/\Delta X$ ratios are constant in time. When the measured mixing ratios of X and Y are plotted in a correlation diagram, all the points should fall on the line defined by equation (A7), which is referred to as the Y-X dilution line in this study.

A.2.2. Case 2: X Is a Long-Lived Species and Y Is a Short-Lived Species

$$\frac{\Delta Y}{\Delta X} = E_{Y-X} \frac{\sum_i \alpha_i e^{-(L_Y + K)t_i}}{\sum_i \alpha_i e^{-Kt_i}} < E_{Y-X} \tag{A8}$$

$\Delta Y/\Delta X$ is smaller than E_{Y-X} because each term in the sum in the numerator is smaller than the corresponding term in the denominator. The $\Delta Y/\Delta X$ ratios decrease with increasing t_i (air mass aging). In a correlation diagram of Y versus X (with X plotted on the horizontal axis), the data from the diluted and aged plumes should lie below the dilution line. The ratio of $\Delta Y/\Delta X$ to E_{Y-X} gives the fraction of Y molecules emitted from biomass burning remaining in the observed air masses.

A.2.3. Case 3: X and Y Are Short-Lived Species

$$\frac{\Delta Y}{\Delta X} = E_{Y-X}\frac{\sum_i \alpha_i e^{-(L_Y+K)t_i}}{\sum_i \alpha_i e^{-(L_X+K)t_i}} \quad \text{(A9)}$$

The $\Delta Y/\Delta X$ ratios should decrease or increase with air mass aging, depending on which species has the larger loss rate. If the loss rates are identical, the $\Delta Y/\Delta X$ ratios should be constant and all the data should stay on one line. By plotting the mixing ratio of Y against several species (X_1, X_2, ...) with known lifetimes, we can estimate the upper/lower limit of the lifetime of species Y. It is important to note that the method does not require knowing the value of E_{Y-X}, because what we need to know is whether the $\Delta Y/\Delta X$ ratios decrease or increase with air mass aging.

A.3. Relative Age

[42] It has been noted that the effects of photochemical and mixing processes on $\Delta Y/\Delta X$ ratios are generally not distinguishable, except for the case of single-puff injection [*McKeen et al.*, 1990, 1996; *Parrish et al.*, 1992; *McKeen and Liu*, 1993]. In spite of this difficulty, however, *McKeen et al.* [1996] have suggested the $\Delta Y/\Delta X$ ratios can still provide a qualitative measure of air mass aging in the sense of the combined influence of photochemistry and mixing processes.

[43] The discussion given in section A.2 basically follows their considerations. As shown by equations (A7)–(A9), the $\Delta Y/\Delta X$ ratio is in general a complex function of elapsed time since emission. An effective time since emission (t^*) can be defined as a weighted average of t_i, $t^* = \sum_i \alpha_i t_i$. However, the observed $\Delta Y/\Delta X$ ratios provide no information on the actual values of α_i that change from air mass to air mass and injection event to injection event. Instead of deriving the effective time since emission (t^*) from the observed values, we define the relative age using a long-lived species X and a short-lived species Y

$$\text{Relative age} = \ln\left(\frac{E_{Y-X}}{\Delta Y/\Delta X}\right) = -\ln\left(\frac{\sum_i \alpha_i e^{-(L_Y+K)t_i}}{\sum_i \alpha_i e^{-Kt_i}}\right). \quad \text{(A10)}$$

The important point is that the relative age is zero for the fresh plumes and increases with time, indicating that it is a qualitative indicator of air mass aging. Note that the relative age depends on which species is chosen as the species X and Y. For a single-injection case ($i = 1$ only),

$$\text{Relative age} = L_Y t_1 = t_1/\tau_Y, \quad \text{(A11)}$$

where τ_Y ($= L_Y^{-1}$) is the photochemical lifetime of Y. In this case, the relative age is the elapsed time since the single-puff emission measured in multiples of the photochemical lifetime of Y.

[44] **Acknowledgments.** The authors express sincere appreciation to D. D. Parrish, S. C. Liu, and I. Simpson for useful comments and discussions. They also acknowledge M. Wheeler, B. Liebmann, and C. A. Smith for providing the OLR data. The BIBLE-B mission was supported by the Earth Observation Research Center, National Space Development Agency of Japan (NASDA/EORC), and by the Japanese Ministry of Education, Culture, Sports, Science and Technology (MEXT).

References

Atkinson, R., D. L. Baulch, R. A. Cox, R. F. Hampson Jr., J. A. Kerr, M. J. Rossi, and J. Troe, Evaluated kinetic, photochemical and heterogeneous data for atmospheric chemistry: Supplement V, *J. Phys. Chem. Ref. Data*, *26*(3), 610–617, 1997.

Blake, D. R., T. Y. Chen, T. W. Smith Jr., C. J.-L. Wang, O. W. Wingenter, N. J. Blake, F. S. Rowland, and E. W. Mayer, Three-dimensional distribution of NMHCs and halocarbons over the northwestern Pacific during the 1991 Pacific Exploratory Mission (PEM-West A), *J. Geophys. Res.*, *101*, 1763–1778, 1996.

Calvert, J. G., R. Atkinson, J. A. Kerr, S. Madronich, G. K. Moortgat, T. J. Wallington, and G. Yarwood, *The Mechanism of Atmospheric Oxidation of the Alkenes*, Oxford Univ. Press, New York, 2000.

Crutzen, P. J., and M. O. Andreae, Biomass burning in the tropics: Impact on atmospheric chemistry and biogeochemical cycles, *Science*, *250*, 1669–1678, 1990.

Crutzen, P. J., L. E. Heidt, J. P. Krasnec, W. H. Pollock, and W. Seiler, Biomass burning as a source of atmospheric gases, CO, H_2, N_2O, NO, CH_3Cl, and COS, *Nature*, *282*, 253–256, 1979.

Fishman, J., J. M. Hoell Jr., R. D. Bendura, R. J. McNeal, and V. W. J. H. Kirchhoff, NASA GTE TRACE-A Experiment (September–October 1992): Overview, *J. Geophys. Res.*, *101*, 23,865–23,880, 1996.

Gery, M. W., G. Z. Whitten, J. P. Killus, and M. C. Dodge, A photochemical kinetics mechanism for urban and regional scale computer modeling, *J. Geophys. Res.*, *94*, 12,925–12,956, 1989.

Gifford, F. A., Horizontal diffusion in the atmosphere: A Lagrangian-dynamical theory, *Atmos. Environ.*, *16*, 505–512, 1982.

Harriss, R. C., et al., The Amazon Boundary Layer Experiment (ABLE 2A): Dry season 1985, *J. Geophys. Res.*, *93*, 1351–1360, 1988.

Hoell, J., et al., Operational overview of the NASA GTE/CITE3 airborne instrument intercomparison for sulfur dioxide, hydrogen sulfide, carbonyl sulfide, dimethyl sulfide, and carbon disulfide, *J. Geophys. Res.*, *98*, 23,291–23,304, 1993.

Hurst, D. F., D. W. T. Griffith, and G. D. Cook, Trace gas emissions from biomass burning in the tropical Australian savannas, *J. Geophys. Res.*, *99*, 16,441–16,456, 1994.

Jacob, D. J., et al., Origin of ozone and NO_x in the tropical troposphere: A photochemical analysis of aircraft observations over the South Atlantic basin, *J. Geophys. Res.*, *101*, 24,235–24,250, 1996.

Kita, K., et al., Photochemical production of ozone in the upper troposphere in association with cumulus convection over Indonesia, *J. Geophys. Res.*, *107*, 8400, doi:10.1029/2001JD000844, 2002. [printed *108*(D3), 2003]

Ko, M., W. Hu, J. Rodriguez, Y. Kondo, M. Koike, K. Kita, S. Kawakami, D. Blake, and S. C. Liu, Photochemical ozone budget during the BIBLE-A and B campaign, *J. Geophys. Res.*, *107*, 8404, doi:10.1029/2001JD000800, 2002. [printed *108*(D3), 2003]

Koike, M., et al., Impact of aircraft emissions on reactive nitrogen over the North Atalantic Flight Corridor region, *J. Geophys. Res.*, *105*, 3665–3677, 2000.

Kondo, Y., S. Kawakami, M. Koike, D. W. Fahey, H. Nakajima, Y. Zhao, N. Toriyama, M. Kanada, G. W. Sachse, and G. L. Gregory, The performance of an aircraft instrument for the measurement of NO_y, *J. Geophys. Res.*, *102*, 28,663–28,671, 1997.

Kondo, Y., et al., Effects of biomass burning, lightning, and convection on O_3, CO, and NO_y over the tropical Pacific and Australia in August–October, *J. Geophys. Res.*, *107*, 8402, doi:10.1029/2001JD000820, 2002. [printed *108*(D3), 2003]

Lary, D. J., A. M. Lee, R. Toumi, M. J. Newchurch, M. Pirre, and J. B. Renard, Carbon aerosols and atmospheric photochemistry, *J. Geophys. Res.*, *102*, 3671–3682, 1997.

Liang, J., L. W. Horowitz, D. J. Jacob, Y. Wang, A. M. Fiore, J. A. Logan, G. M. Gardner, and J. W. Munger, Seasonal budgets of reactive nitrogen species and ozone over the United States, and export fluxes to the global atmosphere, *J. Geophys. Res.*, *103*, 13,435–13,450, 1998.

Liebmann, B., and C. A. Smith, Description of a complete (interpolated) outgoing longwave radiation, *Bull. Amer. Meteor. Soc.*, *77*, 1275–1277, 1996.

Liley, J. B., et al., Black carbon in aerosol during BIBLE-B, *J. Geophys. Res.*, *107*, 8399, doi:10.1029/2001JD000845, 2002. [printed *108*(D3), 2003]

Lindesay, J. A., M. O. Andreae, J. G. Goldammer, G. Harris, H. J. Annegarn, M. Garstang, R. J. Scholes, and B. W. van Wilgen, International geosphere/biosphere programme/international global atmospheric chemistry SAFARI-92 field experiment: Background and overview, *J. Geophys. Res.*, *101*, 23,521–23,530, 1996.

Lovett, G. M., Atmospheric deposition of nutrients and pollutants in North America: An Ecological Perspective, *Ecol. Appl.*, *4*, 629–650, 1994.

Matsueda, H., and H. Y. Inoue, Aircraft measurements of trace gases between Japan and Singapore in October of 1993, 1996, and 1997, *Geophys. Res. Lett.*, *26*, 2413–2416, 1999.

Mauldin, R. L., III, D. J. Tanner, and F. L. Eisele, Measurements of OH during PEM-Tropics A, *J. Geophys. Res.*, *104*, 5817–5827, 1999.

Mauzerall, D. L., J. A. Logan, D. J. Jacob, B. E. Anderson, D. R. Blake, J. D. Bradshaw, B. Heikes, G. W. Sachse, H. Singh, and B. Talbot, Photochemistry in biomass burning plumes and implications for tropospheric ozone over the tropical South Atlantic, *J. Geophys. Res.*, *103*, 8401–8423, 1998.

McKeen, S. A., and S. C. Liu, Hydrocarbon ratios and photochemical history of air masses, *Geophys. Res. Lett.*, *20*, 2363–2366, 1993.

McKeen, S. A., M. Trainer, E. Y. Hsie, R. K. Tallamraju, and S. C. Liu, On the indirect determination of atmospheric OH radical concentrations from reactive hydrocarbon measurements, *J. Geophys. Res.*, *95*, 7493–7500, 1990.

McKeen, S. A., S. C. Liu, E.-Y. Hsie, X. Lin, J. D. Bradshaw, S. Smyth, G. L. Gregory, and D. R. Blake, Hydrocarbon ratios during PEM-WEST A: A model perspective, *J. Geophys. Res.*, *101*, 2087–2109, 1996.

Parrish, D. D., C. J. Hahn, E. J. Williams, R. B. Norton, and F. C. Fehsenfeld, Indications of photochemical histories of Pacific air masses from measurements of atmospheric trace species at Point Arena, *California, J. Geophys. Res.*, *97*, 15,883–15,901, 1992.

Parsons, D. A., M. C. Scholes, R. J. Scholes, and J. S. Levine, Biogenic NO emissions from savanna soils as a function of fire regime, soil type, soil nitrogen, and water status, *J. Geophys. Res.*, *101*, 23,683–23,688, 1996.

Russell-Smith, J., A. Edwards, and G. D. Cook, Reliability of biomass burning estimates from savanna fires: Biomass burning in northern Australia during the 1999 Biomass Burning and Lightning Experiment-B field campaign, *J. Geophys. Res.*, *108*(D3), 8405, doi:10.1029/2001JD000787, 2003.

Saathoff, H., K.-H. Naumann, N. Riemer, S. Kamm, O. Mohler, U. Schurath, H. Vogel, and B. Vogel, The loss of NO_2, HNO_3, NO_3/N_2O_5, and $HO_2/HOONO_2$ on soot aerosol: A chamber and modeling study, *Geophys. Res. Lett.*, *28*, 1957–1960, 2001.

Sander, S. P., et al., Chemical kinetics and photochemical data for use in stratospheric modeling: valuation number 13, *JPL Publ.*, *00–3*, 22–28, 2000.

Sawa, Y., H. Matsueda, Y. Tsutsumi, J. B. Jensen, H. Y. Inoue, and Y. Makino, Tropospheric carbon monoxide and hydrogen measurements over Kalimantan in Indonesia and northern Australia during October, 1997, *Geophys. Res. Lett.*, *26*, 1389–1392, 1999.

Shirai, T., et al., Emission estimates of selected volatile organic compounds from tropical savanna burning in northern Australia, *J. Geophys. Res.*, *108*(D3), 8406, doi:10.1029/2001JD000841, 2003.

Stohl, A., M. Trainer, T. B. Ryerson, J. S. Holloway, and D. D. Parrish, Export of NOy from the North American boundary layer during the 1996 and 1997 North Atlantic Region Experiments, *J. Geophys. Res.*, *107*(D11), 4131, doi:10.1029/2001JD000519, 2002.

Stull, R. B., *An Introduction to Boundary Layer Meteorology*, Kluwer Acad., Norwell, Mass., 1999.

Takegawa, N., et al., Airborne vacuum ultraviolet resonance fluorescence instrument for in situ measurement of CO, *J. Geophys. Res*, *106*, 24,237–24,244, 2001.

Wheeler, M., and G. N. Kiladis, Convectively coupled equatorial waves: Analysis of clouds and temperature in the wavenumber-frequency domain, *J. Atmos. Sci.*, *56*, 374–399, 1999.

D. R. Blake, Department of Chemistry, University of California, 516 Rowland Hall, Irvine, Irvine, CA 92697-2025, USA. (dblake@orion.oac.uci.edu)

W. Hu, Department of Environmental Quality, 629 East Main Street, 8th Floor, Richmond, VA 23219, USA. (whu@deq.state.va.us)

H. Ikeda, Y. Kondo, Y. Miyazaki, and N. Takegawa, Research Center for Advanced Science and Technology, University of Tokyo, 4-6-1 Komaba, Meguro, Tokyo 153-8904, Japan. (hibiki@atmos.rcast.u-tokyo.ac.jp; kondo@atmos.rcast.u-tokyo.ac.jp; yuzom@atmos.rcast.u-tokyo.ac.jp; takegawa@atmos.rcast.u-tokyo.ac.jp)

S. Kawakami, T. Ogawa, and T. Shirai, Earth Observation Research Center, National Space Development Agency of Japan, 1-9-9 Roppongi, Minato-ku, Tokyo 106-0032, Japan. (kawakami@eorc.nasda.go.jp; t_ogawa@eorc.nasda.go.jp; shirai@eorc.nasda.go.jp)

K. Kita, Department of Environmental Sciences, Faculty of Science, Ibaraki University, 2-1-1 Bunkyo, Mito, Ibaraki 310-8512, Japan. (kita@env.sci.ibaraki.ac.jp)

M. Ko, NASA Langley Research Center, Hampton, VA 23681-0001, USA. (m.k.ko@larc.nasa.gov)

M. Koike, Department of Earth and Planetary Science, Graduate School of Science, University of Tokyo, 7-3-1 Hongo, Bunkyo-ku, Tokyo 113-0033, Japan. (koike@eps.s.u-tokyo.ac.jp)

J. B. Liley, National Institute of Water and Atmosphere, Private Bag 50061, Omakau, Central Otago, New Zealand. (b.liley@niwa.cri.nz)

N. Nishi, Department of Earth and Planetary Science, Kyoto University, Sakyo-ku, Kyoto 606-8502, Japan. (nishi@kugi.kyoto-u.ac.jp)

J. Russell-Smith, Bushfire Council of the Northern Territory, Winnellie NT 0821, Australia. (Jeremy.Russell-Smith@plmbay.pwcnt.nt.gov.au)